Remotely Powered Propulsion of Helical Nanobelts

Gilgueng Hwang*, Sinan Haliyo** and Stéphane Régnier**

*Laboratory for Photonics and Nanostructures CNRS, route de Nozay 91460 Marcoussis, France
**Insitut des Systèmes Intelligents et de Robotique, Université Pierre et Marie Curie, 4 Place Jussieu, Paris, France
e-mail: gilgueng.hwang@lpn.cnrs.fr

Abstract—**Nanorobots capable of self-propulsion in low Reynolds number fluids would have a big technological impact in many fields. Few known mechanisms are able to propel such devices. Here we demonstrate that helical nanobelts can swim in liquid when actuated by an electric field generated by electro-osmotic force. Moreover, we show these devices achieve speeds at or slightly above those demonstrated by natural bacteria. The helical nanobelts were designed and fabricated with a head and tail to mimic natural micro-organisms such as bacteria and their flagellae. The electro-osmotic propulsion of helical nanobelts might be used as biomedical carriers, wireless manipulators, and as local probes for rheological measurements.**

I. INTRODUCTION

IN this paper, we describe the design of helical nanobelt (HNB) based nanorobots and demonstrate their electro-osmotic propulsion for in-vivo biomedical applications. Electro-osmotic field propelled HNBs have many potential applications, as biomedical nanorobots targeting and treating cancer cells, or for neural cell probing.

Recently, in-vivo biomedical nanorobots have drawn much interest especially in discovering new and efficient wireless power transfer methods and in controlled locomotion mechanisms. There are many approaches to mimic nature's bacterial swimming behaviors for the locomotion of artificial nanostructures. The swimming of real bacteria is mainly divided into cork-screw type rotating propulsion and the flapping flagella [1]. 30 μm scale bacteria propulsion was demonstrated by an attached ferromagnetic metal pad under an external rotating magnetic field [2-4]. The first rotating magnetic field was used to drive the flagella like tail in [5,6]. Artificial bacteria flagella-like propulsion of helical nanobelts was demonstrated using rotating external magnetic field [2-4]. Further size reduction and applying the same principle to drive artificial bacteria was achieved in [7].

Concerning the driving power source, there are several other limitations of using external field. External field gradient rapidly decreases with the distance from the source.

Therefore, if we consider such limitations, helical propellers should be efficient at low Reynolds numbers [8].

Although the helical morphology is advantageous to enable their propulsion at low Reynolds numbers by reducing the viscous drag, the swimming performance was still much lower than the natural bacteria. To improve the swimming performance, increasing magnetic field intensity could be considered.

However, the major challenges toward their potential in vivo biomedical applications should be noted as the lack of closed loop motion control either by teleoperation or autonomous navigation. This imposes the necessity of localization based on their position tracking. Widely used non-invasive biomedical sensors or imaging devices include radiography, computed tomography (CT), ultrasonography and magnetic resonance imaging (MRI). Considering the realtime navigation and high spatial resolution, MRI has been one of the most promising device among others. Miniaturized objects like 1.5 mm diameter ferromagnetic beads were tracked and navigated under realtime MRI [9]. For the tracking and navigation by MRI of smaller objects at low Reynolds numbers, the addition of the propulsion dedicated field gradient generator in the MRI bore for including propulsion force is necessary. However, as-mentioned gradient coils based propulsion would be largely limited when it has to be used with an external biomedical observation device such as MRI, because of the conflict between the imaging and propelling magnetic fields. Therefore it is inevitable to utilize non-magnetic force propulsion.

As non-magnetic approaches, the flapping or undulating motion of flagella was achieved in meso-scale using a commercial piezoelectric bimorph [10]. Microrobots that harness natural bacteria have also been demonstrated [11-13]. However it still remains unclear which propulsion method is optimal for small scale robotics applications. There are very few works on electric-field based wireless micro/nanorobots. For example, diodes were actuated using electro-osmotic pumping [14, 15]. It showed that electro-osmotic field can be a good candidate for actuating micro/nano robots. However the work was only demonstrated in macro scale. Thus scaling down is
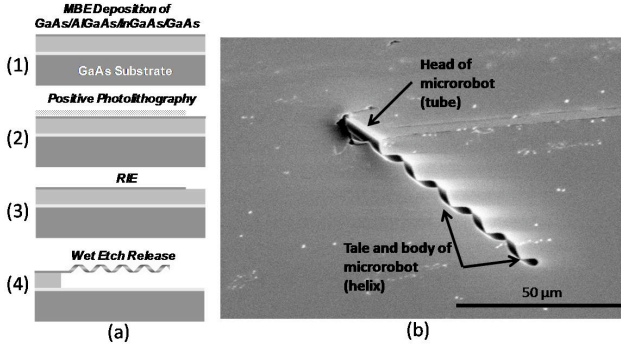
Fig. 1. Basic fabrication process sequence of HNBs (a)(1-4): initial planar bilayer, patterned through conventional microfabrication techniques folds itself into a 3-D nanostructure during wet etch release, (b): created HNB with a tail and a head (SEM photo).

necessary. Furthermore HNBs were not attempted to propel by non-magnetic force.

Therefore in this paper we show a new efficient locomotion method of HNBs by electro-osmotic force. As different types of HNBs showed different swimming performances, we optimized the design of HNBs through the choices of surface material and geometry. The fabrication processes of different types of HNBs are described in next section. The electro-osmotic propulsion experimental setups and the schematics are shown in section 3, and section 4 includes the experimental results of electro-osmotic propulsion of HNBs.

II. FABRICATION OF 3-D HELICAL NANOBELTS

A. Why 3-D Helical Nanobelts?

There are many different types of bacterial locomotion, such as rotating and undulating motions. However, their major features, especially the surface condition, geometry and locomotion, have been evolved to be able to swim efficiently at low Reynolds numbers. Therefore they could survive within extreme environments, such as blood vessels inside the human body. For example, *E. coli* bacteria consist of a highly elastic body formed of protein. Therefore they can self-transform their morphology to increase their swimming velocity in a viscous liquid environment. We consider that such a mobility of natural bacteria is mainly attributed to the nonlinear mechanics of these natural microorganisms.

To mimic such mechanics of natural bacteria, the ultra-flexible nanostructures with large non-constant mechanics are desirable. HNBs are one of the most flexible nanostructures that can be fabricated using standard microfabrication controlled from the geometry design.

Therefore the HNBs used in the paper are well designed for electro-osmotic propulsion by excelling the swimming performance of the natural bacteria. They can also be mass produced by standard microfabrication. Because the process is also controlled, the HNBs with necessary features can be fabricated.

B. Fabrication Process

Figure 1 illustrates the fabrication process. The initial layers were grown on semi-insulating GaAs (Freiberger Compound Materials) using a molecular beam epitaxy system (VEECO, Gen III MBE) equipped with a valved cracker for As and solid sources for Ga and In (Figure 1a). For n-type doping, a solid Si source was used. Substrate temperature was measured by a pyrometer. After a thin GaAs buffer layer, the 500 nm thick sacrificial AlGaAs layer is deposited. The layer contains 20% Ga in order to prevent oxidation. The sacrificial layer in previous designs was made of AlAs. The oxidation of these layers after exposure damaged the InGaAs/GaAs bilayer. On top of the sacrificial layer the InGaAs/GaAs layer is deposited which later self-forms into the nanosprings. An In content of 15% in the InGaAs layer was determined by X-ray diffraction (XRD) measurements. The thickness of this layer must be smaller than the critical thickness to maintain elastic strain. The layer properties along with other specifications of the structures are summarized in Table 1. During the deposition of the InGaAs/GaAs bilayer on this wafer, we attempted to get a slightly lower doping concentration than on the wafer that was used for HNB 2, 3 and 4. From the results it seems that the doping concentration was too high which resulted in a partial self-compensation and, therefore, in a decrease in the effective doping concentration. The doping concentrations of the structures are 4.4×10^{18} cm^{-3} and 8.5×10^{18} cm^{-3} (Table 1).

The initial pattern can be created through photolithography. Reversible photoresist AZ5214 was used as a resist. After the development of the resist, ion etching (RIE) with a SiCl$_4$ gas was used to transfer the pattern to the InGaAs/GaAs bilayers [16]. For HNB 4, the thickness of photoresist was reduced around 50 nm with O$_2$ plasmas. For metallic HNB 3, the Cr/Ni layers on the surface and on the heads to which the structures are fixed at the end were created before RIE through a lift-off process with negative photoresist AZ5214.

The Cr layer is 10 nm thick and serves as an adhesion layer. The 10 nm thick Ni layer is used for metal HNB 3.

TABLE I
SPECIFICATIONS OF HELICAL NANOBELTS USED IN EXPERIMENTS AND SIMULATIONS

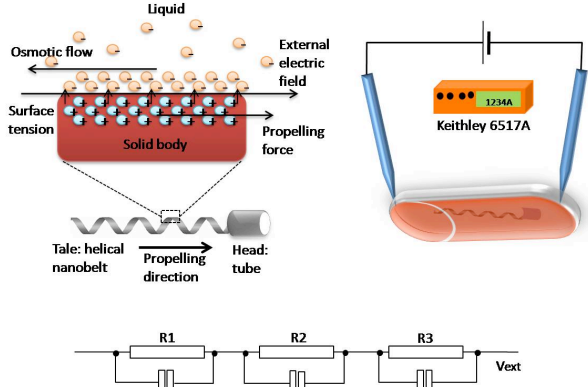|	HNB 1 low	HNB 2 high	HNB 3 Cr/Ni	HNB 4 Dielectric
Thickness In$_{0.15}$Ga$_{0.85}$As/GaAs	11.6 / 15.6 nm	8 ~ 10 /15.6 nm	11.6 / 15.6 nm	
Thickness Cr/Ni	NA		10 / 10 nm	Photoresist ~ 50
Diameter (tail=head)	2.1 μm			
Pitch & width (tail)	14 μm & 2.5 μm			
Number of turns (tail)	4.5 turns			
Length (head)	12 μm			
Length (total)	74 μm			
InGaAs/GaAs Doping (N_D)	$4.4 \cdot 10^{18}$ cm^{-3}	$8.5 \cdot 10^{18}$ cm^{-3}		

Fig. 2. Schematic diagrams of the experiments for HNB swimming. A DC bias was applied between two electrodes located through axial direction of HNB body. Thus the propulsion direction can be controlled and predicted by the configuration of electrodes. For controlling the direction of electric field, micromanipulators with tungsten probes were utilized to form electrodes.
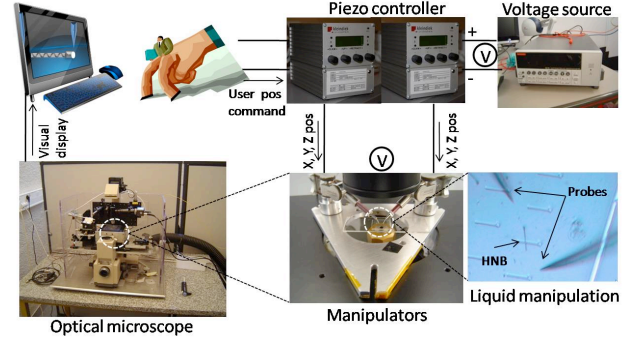

Fig. 3. System setup for electro-osmotic propulsion experiments: Optical microscope with a camera was used to give user visual feedback and thus proper manipulation in liquid. User operates the piezo controller to manipulate tungsten probes, which were utilized to manipulate HNBs and to apply electric field generated by an external voltage source.

Finally, a 2% HF aqueous solution at 4°C was used to selectively etch the AlGaAs sacrificial layer under the InGaAs/GaAs heterostructures for the self-forming of the nanostructures (Figure 1a). During this wet etch, the patterned bilayer curled up along a <100> direction releasing the internal strain and forming 3-D structures. The direction of the scrolling is determined by the anisotropy in stiffness of the InGaAs/GaAs bilayer. After the wet etch release, the chips were rinsed in deionized water and subsequently in isopropyl alcohol [17]. Samples are also conserved in isopropyl alcohol in order to prevent oxidation by water of heads to which the structures are fixed.

As a result, four different types of HNBs (metal, high, low doping and dielectric HNBs) with similar geometry features were created based on the described process (Figure 1b). The detailed specifications of each HNB are summarized in the Table 1.

III. ELECTRO-OSMOTIC FORCE PROPULSION

In this section, the basic principle and experimental setup to generate electro-osmosis effect is described.

A. Principle of HNB Electro-osmotic Propulsion

The propulsion of HNBs involves two conversions: transforming energy from an external source to a force, and transforming this force into a motion. The proposed method to supply power remotely to nanorobots is the electrokinetic process. Its main advantage for in-vivo applications is its compatibility with medical Magnetic Resonance Imaging.

In general, the surface charge that develops at the solid-liquid interfaces plays an important role in a number of electrokinetic processes. Due to the presence of a thin interfacial layer named the Stern layer, it results in a non-zero electric potential at the liquid interface, also known as the zeta potential ζ. This potential is screened by mobile counter-ions diffusing in the liquid in a layer generally named Electrical Diffuse Layer (EDL), which has

a typical thickness of a few tens of nanometers depending on the solution ionic strength. Under an electric potential difference, the resulting electric field puts in motion the excess counter-ions in the EDL. This moving layer drags the whole liquid inside the fluidic medium, resulting in "plug-like" flows also referred to as Electro-Osmotic Flows (EOF). In addition, one should also consider the surface charge developing at the HNB surface. In the case of a nanorobot floating in liquid, its own Stern layer generates a flow which applies a hydrodynamic pressure on the surface of the robot, propelling it in the opposite direction.

Figure 2 depicts the electro-osmotic propulsion mechanism through the interface between HNB`s thin membrane surface and liquid medium solution. Since the propulsion force occurs through the whole surface, the large surface to volume ratio of HNBs is very advantageous.

We proved that the HNB motility results from a local electro-osmotic flux powered by the external field. The specific direction of HNB`s propulsion along the cathode and anode probes indicates that a DC field along the HNB is responsible for this propulsion. The equivalent circuit can predict that the electro-osmotic propulsion force is affected by the difference of electrical resistivity between the medium solution and the HNB (Figure 2). The electric voltage applied to the HNB by the external field can be estimated from a serially-connected resistors model describing the ionic conductance through the liquid medium, and capacitors for the ionic layers. In a DC electric field, the resistance is the leading contribution. The resulting DC voltage of magnitude V_d induced in the HNB is modeled as

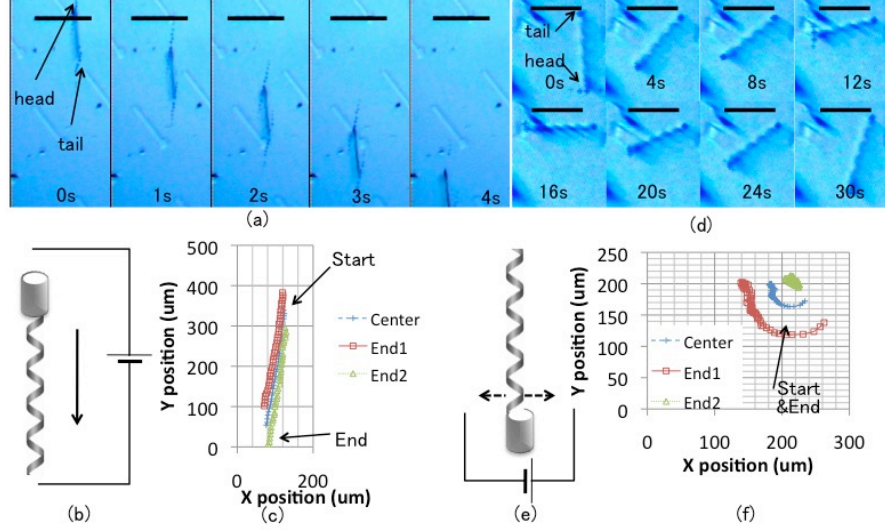$$V_d = \frac{R_2}{R_1 + R_2 + R_3} V_{ext} \tag{1}$$

Fig. 4. Different swimming propulsions of HNBs are achieved by modifying electrode's configuration. Series of snap shots during backward (a) and rotating, (d) propulsions were taken during the experiments (b and e). The trajectories of each swimming experiment are displayed in (c) and (f). The scale bars in (a) and (d) are 80 µm and 60 µm.

Where V_{ext} is the DC input voltage applied to the probes in the petri-dish and R_1 (resistance between left electrode and HNB), R_2 (resistance of HNB), R_3 (resistance between HNB and right electrode) are depicted in Fig. 2. Assuming that the resistance of the liquid is linearly proportional to the distance between the probes, equation (1) can be simplified as $V_d = E_{ext}l_d$, where l_d is the length of the HNB body and E_{ext} is the external DC field. The external DC field between the electrodes makes electro-osmotic fluid flow along the HNB body.

We consider a liquid electrolyte, consisting of positive and negative particles in liquid solution. The interface between the electrolyte and the container wall generally forms a double layer in equilibrium, where a nonzero surface charge is screened by a very thin diffuse layer of excess ionic charge of width λ, the Debye screening length (typically 1-100nm). The double layer is effectively a capacitor skin at the interface, which has a small voltage ζ across called the zeta potential. We describe the effect of the HNB and also the environment under electric field more clearly by further detailed model which decomposes the part of intrinsic electrophoretic force directly generated to HNB and the electro-osmotic flow from the surface interaction. Now we can consider a tangential electric field E_{ii} applied in parallel to a flat surface. The electric field acts on ions in the diffuse part of the double layer, which drag the fluid to produce an effective slip velocity outside the double layer by the Helmholtz-Smoluchowski formula (Eq. 2) [18],

$$u_{11} = \left(\frac{2\varepsilon_0\varepsilon_r \zeta_{HNB} H}{3\eta} - \frac{\varepsilon_0\varepsilon_r \zeta}{\eta} \right) \vec{E} \qquad (2)$$

where $\varepsilon_0\varepsilon_r$ and η are the electrolyte permittivity and fluid viscosity, which are constants (environment parameters). Increasing the speed of the HNB requires to increase ζ_{HNB}

and H which are the zeta potential around the surface of the HNB and the Henri function, which depends on the geometry and hydrodynamic properties, and the external field (E). The Zeta potential ζ on the borders of the surface is inversely proportional to the speed, thus it can be minimized and controlled by applying experiments under closed microfluidic channel.

An important application of electro-osmotic flow is capillary electro-osmosis, where an electric field is applied down a capillary tube to generate an uniform plug flow (Eq. 2), driven by the slip at the surface. Typical flow speeds of 100 µm/s (6 mm/min) are produced by a field of 100 Volt/cm. This value will be used to compare the swimming performance of HNBs in the next section. It should be noted here that the electro-osmotic propulsion does not depend on the size of the micro-robots. Thus microscopic HNB could move about as fast as a macrosized one.

For the experiments in this paper, we used isopropyl alcohol as medium solution to minimize the possible aging effect or oxidation of HNBs by water. However, the relation between swimming performance and medium solution's pH and/or resistivity is not explored here.

B. Electro-osmotic Propulsion Experimental Setup

To cut and release the fixed end of HNBs from chips and generate electric field through the liquid medium and HNBs, at least two probes with high precision positioning accuracy are required. Every experiment is monitored and recorded for the later analysis of the swimming performances of HNBs. Therefore multiple nanorobotic manipulators are installed under the optical microscope. The complete experimental setup is shown in Figure 3. Two nanorobotic manipulators (Kleindiek, MM3A) are installed under optical microscope; each has three degrees of freedom, and respectively 5 nm, 3.5 nm, and 0.25 nm resolutions in X, Y,

and Z directions. For the application of the electrical field and high resistance measurement, an electrometer with a DC power supply (Keithley 6517A) was used. Two probes attached to each side of manipulators are positioned in less than 1mm distance. To avoid the optical reflection from the meniscus between probes and liquid medium interface, longer probes (~5mm) with sharp tips were used.

IV. ELECTRO-OSMOTIC PROPULSION EXPERIMENT

A. Propulsion Experiment by Electro-osmotic Pump

Figure 4a describes the series of photos taken from the recorded video and the tracked HNB`s trajectories in forward propulsion. An external DC field of 118 V/mm was applied for the forward propulsion and results in backward motion in negative potential. The velocity achieved with this field and configuration is 126 µm/s, which exceeds the propulsion velocity of E. coli bacteria with a rotating frequency of 100 Hz [19,20]. Since the size of HNBs and natural bacteria (e.g. E. coli bacteria) are different (HNB is 10 times larger than E. coli), relative velocities were compared using units of body-length.

Through the experiments at an electric field of 239 V/mm, a velocity of 1,785 µm/s is achieved with HNBs, which is 24 body-lengths per second. It should be noted that E. coli bacteria moves at a speed around 10 body-lengths per second [19].

B. Controlled Swimming Experiments of HNBs

Figure 4 demonstrates the forward and rotating propulsion of HNBs. Experiments are depicted in Fig. 4b and e. The probes attached to manipulators can change the configuration to generate the desired electric field gradient. Please note that the rotation was achieved using a HNB fixed in one extremity while the other is free. In this case, the electrode configuration was fixed to make the HNB rotate. The head was fixed with van der waals interaction with the surface. Therefore this surface interaction can be reversibly reduced to release HNBs from substrate by applying a small amount of mechanical force using a manipulator. Furthermore, the forward and backward swimming direction can be converted without the complicated tumbling motion of E. coli bacteria [20]. The swimming propulsions of HNBs are achieved by modifying the electrodes` configuration. A series of snap shots during forward (Figure 4a) and rotating (Figure 4d) propulsions were taken during the propulsion experiments. The trajectories of each swimming experiment are displayed in Fig. 4c and 4f. For trajectories, a video analysis software and a custom-made C++ program were utilized. Rotation of HNBs was achieved by their aligning to the applied field direction.

We have confirmed that HNBs swimming directions could be easily controlled by differentiating the field gradient. For the steering control, the field gradient needs to be aligned to the rotational axes of the HNBs. The high surface-to-volume ratio of HNBs increases the swimming efficiency by increasing the charged area in a given volume and mass.

The maneuverability of the currently demonstrated electro-osmotic HNBs is still limited to the basic motions compared to the magnetic field based approaches. However it can be overcome by making addressable swimming using an array of embedded electrodes.

In the paper, one side of the HNB was fixed to the substrate and the other side was free to demonstrate the rotation. Of course the rotation of a non-tethered HNB is also possible. Recently, shark-like motion and rotation motion have also been demonstrated. By controlling the field gradient in more detail, the maneuverability of a HNB can be further improved.

C. Force Estimation

We estimate the force generated by the HNB`s swimming from the drag it overcomes, considering its shape approximately as an ellipsoid [7].

$$F = \frac{4\eta\pi a v}{\left[\ln\left(\frac{2a}{b}\right) - \frac{1}{2}\right]} \tag{3}$$

where a and b are the dimensions along the longitudinal and lateral axes respectively, η is the viscosity of the liquid medium, and v is speed of the HNB. For a 74 µm long HNB with a diameter of 2.1µm moving at 1.8 mm/s in isopropyl alcohol medium, the generated force of 1.3 nN (Eq. 3) is an order of magnitude higher than the conventional optical trap force which is less than 200 pN. Furthermore, HNBs can apply a large pressure, approximately 91 N/m², which can be advantageous used for local manipulation, such as on biological membranes [18,19].

D. Swimming Performances of Different HNBs

We analyzed the swimming performances of different HNBs as a function of the parameters controlling the electro-osmotic propulsion force. The maximum velocity of an HNB in isopropyl alcohol medium as a function of electric field intensity is characterized in Fig. 5. A 74 µm long HNB is used for the tests. The intensity of the field is increased from 24.99 to 239.66 V/mm. The maximum velocity was not linearly proportional to the applied field intensity, especially at higher field intensity above 87.75 V/mm. This can be explained by the fact that HNBs swimming in isopropyl medium have relatively higher Reynolds numbers in this region compared to the water. Reynolds number can be calculated by the equation [1].

$$R_e = \frac{L v \rho}{\mu} \tag{4}$$

Where L is the length of HNB, v is the velocity, ρ is the density of the liquid and μ is the viscosity of the liquid. For
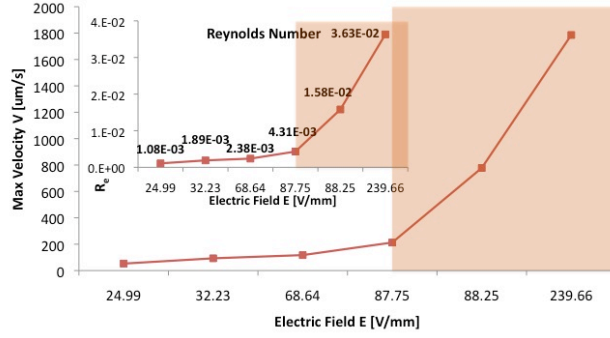
Fig. 5. Dependence of HNB velocity on applied electric field intensity. The plot was obtained during the swimming experiments of a 74 μm long HNB in isopropyl alcohol medium. The nonlinearity of the swimming performance is demonstrated at the region with higher electric field intensity than 87.75 V/mm. The inset figure shows the Reynolds numbers in different velocities *vs.* applied electric field.

isopropyl alcohol, the kinematic viscosity (μ/ρ) is approximately 3.6×10^{-2} cm^2/s thus the Reynolds number is proportional to the length and velocity of the HNB. In natural bacterial propulsion with 1 μm length and a velocity of 30 μm/s, the Reynolds number is 3×10^{-5} in water [1]. For example, 74 μm long HNBs swimming at 1,785 μm/s in isopropyl alcohol medium have a Reynolds number of 3.6×10^{-2}, which is much higher than bacterial propulsion. It involves more inertial effect during the propulsion and explains the non-linearity of the velocity and electric field. In our experiments, the swimming velocity of HNBs is between 4.4 μm/s and 1,785 μm/s. The Reynolds numbers are thus between 3.3×10^{-4} and 3.6×10^{-2}. Fig. 5 and the inset plot depict the Reynolds numbers of HNBs with different velocities. It is apparent that the linear relation between the field intensity and the velocity is achieved with a velocity less than 87.75 V/mm and Reynolds numbers around 4.3×10^{-3}. All other previous bacteria-like propulsions were demonstrated within this velocity around 200 μm/s [3,4,7]. This number could be at the marginal limit representing natural bacterial propulsion. The unusually fast swimming propulsion demonstrated in this work is due to the generated inertial force to overcome the viscous drag by reaching at a higher Reynolds numbers. The inertial effect of a rigid-body swimmer at low Reynolds number is tiny so ignorable. According to the speculation based on empirical experiments, however the extremely flexible HNBs (the stiffness of HNBs can be around 0.001 N/m and 0.00001 N/m in longitudinal and bending respectively) can reduce the viscous drag by oscillating the HNB. Therefore they can undergo the inertial effect. In fact, the HNB continued to swim for a while even though the field was cut off when it is accelerated to a velocity faster than the critical velocity. This deformation can generate the surface charges of HNBs to enhance local electro-osmotic force. The HNBs showed the giant piezoresistivity partly due to the piezoelectric effect [17]. Therefore the surface charge added the induced propulsion force thus contributed to the nonlinear curve of
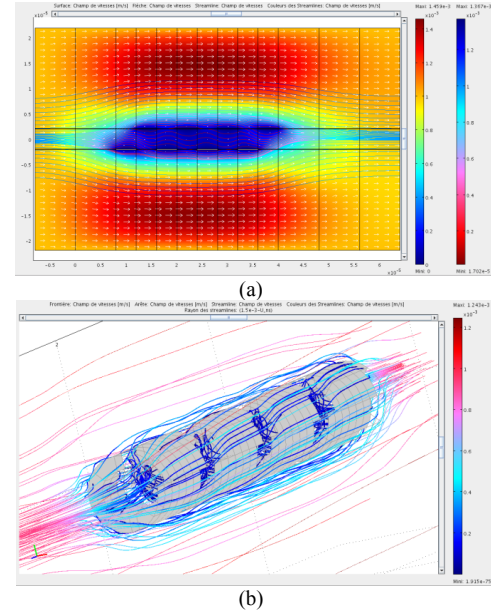

(a)

(b)

Fig. 6. Hydrodynamic simulations using finite element modeling: (a) 2-D stream around HNB, (b) coarse 3-D model around HNB.

the maximum velocity. It can explain the continued swimming phenomenon even after external field is cut off.

Furthermore, the non-linearity and fluctuations of the curve in Figure 5 are also attributed to intermolecular interactions of the HNB with the substrate. Especially the heavier tube type heads of HNBs were apt to submerge more than the body and tail, which makes the initial energy to break this interaction difficult to predict.

To explain the unusually fast swimming HNB, finite element simulations in liquid medium were performed. Figure 6a shows the cross-sectional view of the HNB moving with a velocity of 1 mm/s. Although the inside of HNB is a bit undulated, a very regular laminar flow was estimated around it. As was expected, the flow speed was slower inside of HNB and was faster outside. This laminar flow is due to the helical morphology with ultra-thin layers of HNB, even though the flow speed was fast for the given dimensions. The Reynolds number was around 10^{-2}, which acts like a very viscous liquid. To further estimate the undulation inside the HNB, a 3-D model of a HNB was created from the assembled hexahedral blocks (Figure 6b). This coarse model reduces the calculation time of the finer model. The same phenomena with a very slower laminar flow inside and a faster one outside HNB were estimated. In this case, the flow inside HNB was winded slowly. This reveals that the fast swimming HNB can generate inner torque thus rotates the structure to balance the energy. The rotation energy contributes to keep the flow around HNB very laminar while it swims very fast. Therefore, it is predicted that swimming performance would highly depend on the surface geometry, especially inside the HNB.

To further understand the repeatable swimming behaviors due to an electro-osmotic force and to find the
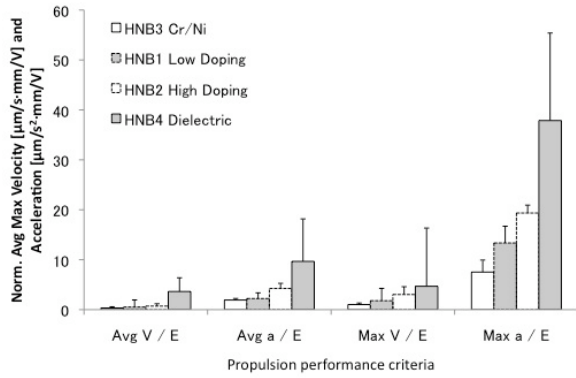
Fig. 7. Dependence of normalized velocity and acceleration of propulsion on 4 types of HNBs. High and low doped semiconductor HNB showed higher swimming performance than metal (Cr/Ni) coated HNB and best performances are achieved with type 4 (Dielectric).

TABLE II
PROPULSION PERFORMANCE COMPARISON OF HELICAL STRUCTURES

	Magnetic 1 [3,4]	Magnetic 2 [7]	**Electro-osmotic**	E. Coli [16,17,20]
Length / Diameter [μm]	50 / 2.8	2 / 0.2	**74 / 2.1**	2 / 0.5
Max. Vel. [μm/s]	18	40	**1785**	20
Body-length / second	0.4 ×	20 ×	**24 ×**	10 ×
Force [pN]	3.0	~ 1.0	**1300**	0.6

optimized design parameters, especially the surface profile, four different types of HNB, performance was investigated were evaluated in their performances. High and low doping HNB, a metallic (Cr/Ni) one and a dielectric counterpart were analyzed. Figure 6 shows the average and maximum propulsion velocity and acceleration normalized by the applied electric field. HNB performance was investigated in several steps (6 - 11 steps) ranging from 24 to 401 V/m. It was difficult to compare four HNB in identical single field intensity because the experimental configuration of probes and HNB are difficult to maintain in-between each experiment. Therefore, a statistical average velocity was chosen to describe the general behavior of different HNB. It should also be noted that experiments on different types of HNB were conducted in different days which might slightly change electrical resistivity of the liquid medium. Even though the exact resistance values of the utilized HNBs were not verified because of the difficulty in collecting them after experiments, the intrinsic resistance of HNB can be predicted as $R_{HNB4} > R_{HNB1} > R_{HNB2} > R_{HNB3}$. Hence, the average and maximum velocities and accelerations depend on the resistance of HNB as was expected from the equation (3). Highly doped HNB2 showed better swimming performance than low doped HNB1. This can be explained by the fact that the InGaAs layer thickness (estimated as 8 ~ 10 nm) of HNB2 is slightly thinner than the one of HNB1 (11 nm). It results in better performance in HNB2 than HNB1 from the reduced gravity effect and hydrodynamic friction regardless of the higher conductivity. It reveals that the doping concentration does not play much role in the swimming performance compared to the geometry or volume effect. It should also be noted that the HNB3 and HNB4 are slightly thicker than HNB1 and HNB2 because of additional metallic layers (Cr/Ni 10/10nm, AZ5214 photoresist around 50 nm, Table 1). However, the HNB3 had lower performance while HNB4 was better than the others. In the case of HNB3, this can be explained by the increase in hydrodynamic friction during swimming which

slow down HNB. Furthermore, in case of metallic HNB3, the gravitational force can also increase the surface interaction force by dragging it down to the substrate. The detailed calculation and comparison of buoyancy force and gravitational force are not described here, however the resulting nonfluidic forces (as the difference between the gravitational force and the buoyancy force) on HNB3 is 0.94 pN, which is two times higher than on HNB1 (0.43 pN). These negative effects on HNB3 reduce its swimming performance compared to the others (Figure 7). The result of HNB4 is contrary to the HNB3 while additional layer was deposited onto the surface. It can be explained by the fact that the nonfluidic force of HNB4 was decreased by the increased buoyancy force from the photoresist, which has much lower density than both gold and nickel.

The result clearly shows the high dependency on the surface charge and thus zeta potential in dielectric surface coating to HNB compared to conductive or semiconductor materials (Figure 7).

Finally the swimming performance of electro-osmotic propulsion HNBs was compared with other helical nanostructures (Table II). Compared to two rotating magnetic propulsions of helical nanostructures, the demonstrated electro-osmotic propulsion of HNBs showed much higher swimming performance in terms of maximum swimming velocity and manipulation force. Furthermore it even excels the one of natural E. coli bacterial propulsion. The demonstrated velocity (1785 μm/s) can reach 90 times faster than others. Concerning to the manipulation force reaching at around 1.3 nN, it is 1,000 times higher than others. It is even much higher than widely used optical tweezers (~ 200 pN). The swimming efficiency can further be improved by further size reduction and/or surface coating with dielectric materials.

The absolute voltage applied in the work ranges from a few volts to a few tens of volts and it limits their biomedical applications in this form. However it should be noted here that the electro-osmotic swimming propulsion was demonstrated in the open channel more precisely in the petri-dish. Therefore all experiments in this type of open channel assume certain amount of offset voltage compared to the experiments in a tiny closed channel.

In the case of a closed channel, like a human blood vessel, the propulsion force can further be enhanced by the

reduced gravitational force thus increasing buoyancy force. Furthermore the surface interaction from the petri-dish can be minimized as well in case of the closed channel experiments. We are currently working on HNB swimming inside a microfluidic channel for controlling the swimming environment.

For in-vivo biomedical applications of the electro-osmotic HNB swimmers, non-invasive and external electric field generation is inevitable. As one of solutions, patch-type external embedded electrodes can be considered to control the swimming motions of HNBs remotely.

V. Conclusion

The demonstrated direct pulling of HNBs by electro-osmotic pumping was proven to be an efficient energy conversion mechanism for microscopic artificial swimming objects and overcomes easily the viscous drag and gravitational forces in an aqueous environment at low Reynolds numbers. Swimming velocities as fast as 1.8 mm/s (24 times the body length per second) and pushing forces as high as 1.3 nN are achieved by HNBs propelled by an electro-osmotic force under an external electric field. These performances are higher than other state-of-the-art microscale artificial swimmers. Please note that the velocity of 24 body lengths per second is even faster than natural bacterial propulsion. An inertia effect was observed above a critical velocity, and was speculated as the reason why the electro-osmotic HNB swimmers could outrun natural bacteria. Hydrodynamic simulation of this unusually fast swimmer revealed a very laminar flow around the HNB with a torque inside them. Although helical morphology with a thin-film is beneficial to such a fast swimming at low Reynolds numbers, the swimming performance appears to depend highly on the surface conditions. Among the four different types, dielectric polymer coated HNB showed the best swimming performance compared to others with metallic or semiconductor surfaces. These HNB can be used as wireless liquid manipulators and assemblers for biomedical or MEMS/NEMS applications or remote physical or chemical detection by functionalizing with proper read-outs. For these complex tasks, it would be necessary to improve the control schemes and methods, implemented through finer hydrodynamic finite element model simulations.

References

[1] E. M. Purcell, "Life at Low Reynolds Number," in *American Journal of Physics,* vol. 45, 1977, pp. 3–11.

[2] D. J. Bell, S. Leutenegger, K. M. Hammar, L. X. Dong, B. J. Nelson D. X. Dong, "Flagella-like Propulsion for Microrobots Using a Magnetic Nanocoil and Rotating Electromagnetic Field." in *IEEE International Conference on Robotics and Autumation*, 2007, pp. 1128–1133.

[3] L. Zhang, J. J. Abbott, L. Dong, B. E. Kratochvil, D. Bell, B. J. Nelson, "Artificial Bacterial Flagella: Fabrication and Magnetic Control" in *Applied Physics Letters*, vol. 94, no. 6, 2009, pp. 064107-3.

[4] L. Zhang, J. J. Abbott, L. Dong, K. E. Peyer, B. E. Kratochvil, H. Zhang, C. Bergeles, B. J. Nelson, "Characterizing the Swimming Properties of Artificial Bacterial Flagella" in *Nano Letters*, vol. 9, no. 10, 2009, pp. 3663–3667.

[5] T. Honda, K. I. Arai, K. Ishiyama, "Micro swimming mechanisms propelled by external magnetic fields," in *IEEE Transactions on Magnetics*, vol. 32, no. 5, 1996, pp. 5085–5087.

[6] K. Ishiyama, K. I. Arai, M. Sendoh, A. Yamazaki, "Spiral-type micro-machine for medical applications," in *Journal of Micromechatronics*, vol. 2, no. 1, 2003, pp. 77-86.

[7] A. Ghosh, P. Fischer, "Controlled Propulsion of Artificial Magnetic Nanostructured Propellers," in *Nano Letters*, vol. 9, no. 6, 2009, pp. 2243-2245.

[8] J. J. Abbott, K. E. Peyer, M. C. Lagomarsino, L. Zhang, L. Dong, I. K. Kaliakatsos, B. J. Nelson, "How Should Microrobots Swim?," in *International Journal of Robotics Research*, doi: 10.1177/0278364909341685.

[9] S. Martel, J. Mathieu, O. Felfoul, A. Chanu, E. Aboussouan, S. Tamaz, P. Pouponneau, L. Yahia, G. Beaudoin, G. Soulez, M. Mankiewicz, "Automatic navigation of an untethered device in the artery of a living animal using a conventional clinical magnetic resonance imaging system," in *Applied Physics Letters*, vol. 90, 2007, pp. 114105.

[10] G. Kosa, P. Jakab, N. Hata, F. Jolesz, Z. Neubach, M. Shoham, M. Zaaroor, G. Szekely, "Flagella Swimming for Medical Micro Robots: Theory, Experiments and Application," in *IEEE International Conference on Biomedical Robotics and Biomechatronics*, 2008, pp. 258–263.

[11] S. Martel, C. Tremblay, S. Ngakeng, G. Langlois, "Controlled manipulation and actuation of micro-objects with magnetotactic bacteria," in *Applied Physics Letters*, vol. 89, 2006, pp. 233904.

[12] B. Behkam, M. Sitti, "Bacterial flagella-based propulsion and on/off motion control of microscale objects," in *Applied Physics Letters*, vol. 90, no. 2, 2007, pp 1-3.

[13] E. Steager, C. B. Kim, C. Naik, J. Patel, S. Bith, L. Reber, M. J. Kim, "Control of microfabricated structures powered by flagellated bacteria using phototaxis," in *Applied Physics Letters*, vol. 90, no. 26, 2007, pp. 263901.

[14] S. T. Chang, V. N. Paunov, D. N. Petsev, O. D. Velev, "Remotely Powered Self-propelling Particles and Micropumps based on Miniature Diodes," in *Nature Materials*, vol. 6, no. 3, 2007, pp. 235-240.

[15] S. T. Chang, E. Beaumont, D. N. Petsev, O. D. Velev, "Remotely powered distributed microfluidic pumps and mixers based on miniature diodes," in *Lab on a Chip*, vol. 8, 2008, pp. 117-124.

[16] S. Varoutsis, S. Laurent, I. Sagnes, A. Lemaitre, L. Ferlazzo, C. Mériadec, G. Patriarche, I. Robert-Philip, I. Abram, "Reactive-ion etching of high-Q and submicron-diameter GaAs/AlAs micropillar cavities," in *Journal of Vacuum Science and Technology B*, vol. 23, no. 6, 2005, pp. 2499-2503.

[17] G. Hwang, D. J. Bell, L. Dong, H. Hashimoto, S. Schon, B. J. Nelson, "Piezoresistive InGaAs/GaAs Nanosprings with Metal Connectors," in *Nano Letters*, vol. 9, no. 2, 2009, pp. 554–561.

[18] R. J. Hunter, "*Zeta potential in colloid science principles and applications*," Academic Press, London a.o., 1981.

[19] H. C. Berg, D. A. Brown, "Chemotaxis in Escherichia coli analysed by Three-dimensional Tracking," in *Nature*, vol. 239, no. 5374, 1972, pp. 500–504.

[20] H. C. Berg, "*E. coli in Motion*," Springer, New York, 2004.

[21] W. C. Little, M. L. Smith, U. Ebneter, V. Vogel, "Assay to mechanically tune and optically probe fibrillar fibronectin conformations from fully relaxed to breakage," in *Matrix Biology*, vol. 27, 2008, pp. 451-461.

[22] S. J. Park, M. B. Goodman, B. L. Pruitt, "Analysis of nematode mechanics by piezoresistive displacement clamp," in *Proceedings of the National Academy of Science of the United States of America (PNAS)*, vol. 104, 2007, pp. 17376-17381.

[23] S. Chattopadhyay, R. Moldovan, C. Yeung, X. L. Wu, "Swimming efficiency of bacterium Escherichia coli," in *Proceedings of the National Academy of Science of the United States of America (PNAS)*, vol. 103, 2006, pp. 13712-13717.